Penetration length of ferrosmectics

C. Quilliet, P. Fabre, M. Veyssié

Classification
Physics Abstracts
61.30 — 82.70D — 75.50M

Penetration length of ferrosmectics

C. Quilliet, P. Fabre and M. Veyssié

Laboratoire de physique de la matière condensée (*), Collège de France, 11 pl. M. Berthelot, 75231 Paris Cedex 05, France

(*Received 14 April 1993, accepted 4 June 1993*)

Résumé. — Nous avons effectué les premières mesures de la longueur de pénétration smectique $\lambda = \sqrt{K/\bar{B}}$ (K et $\bar{B}$ étant respectivement les constantes élastiques de courbure et de compression) sur des ferrosmectiques, qui sont des smectiques lyotropes dopés, et ce par une méthode utilisant l'observation des défauts créés dans une cellule d'épaisseur variable. En particulier, nous avons déterminé l'évolution de λ avec la concentration ϕ en particules dopantes. Les résultats principaux sont que λ reste constant pour des petites valeurs de ϕ, puis diminue, et ceci d'autant plus rapidement que la phase est gonflée. Nous discutons ces résultats et leurs conséquences sur les variations de K et $\bar{B}$; ceux-ci confirment et complètent une précédente étude de ces phases par diffusion de neutrons. Nous avons également observé des dislocations coin de très petit vecteur de Burgers, dont l'existence dans cette géométrie n'était pas envisagée pour des phases gonflées ; nous proposons un modèle microscopique pour évaluer λ à partir de ces dislocations.

Abstract. — We report the first quantitative measurements of the smectic penetration length $\lambda = \sqrt{K/\bar{B}}$, with K and $\bar{B}$ the curvature and compression elastic constants, for ferrosmectics, which are doped lyotropic smectics. We use a method based on the observation of defects created in a cell of varying thickness. In particular, we determine the evolution of λ with the volume fraction of doping particles, ϕ. The main experimental features are that λ is constant at small ϕ then decreases, and that this diminution is enhanced at large swelling of the phases. The results and their consequences on K and $\bar{B}$ are discussed ; they support and complement previous neutron scattering studies. We also observe edge dislocations with very small Burgers vector, that were not expected in such swollen phases. A microscopic model is proposed to evaluate λ from such defects.

1. Introduction.

Amphicolloids, which are lyotropic mesophases doped with solid colloidal particles, have been recently made [1, 2]. Amongst them, the *ferrosmectics* are swollen smectic phases containing magnetic particles, the size of which is comparable to the smectic periodicity.

(*) URA CNRS n 792.

These hybrid systems, that arise as strata of ferrofluid separated by lyotropic membranes, have many novel properties, the most spectacular one being a reorientation of the smectic matrix under a magnetic field [1, 3]. The physics of such phases involves both the magnetic properties of the particles and the elastic properties of the smectic. Here we are interested in the elastic properties of these systems, mainly described by the compression constant of the smectic, $\bar{B}$, and the curvature elastic constant K, and in the evolution of these quantities with the volume fraction of the particles ϕ. Theoretical and experimental studies of the elastic features of smectic liquid crystals have been extensively performed, concentrating in the last few years on lyotropic membranar assemblies [4]. In this paper, we study a characteristic length closely related to the elasticity of the system : the smectic penetration length λ [5] defined by :

$$\lambda = \sqrt{K/\bar{B}} \,. \tag{1}$$

Physically, a deformation of wavevector q (parallel to the layers) decays on a length scale $1/\lambda q^2$; a high value of λ is then the indication of a « soft » smectic. In order to determine this smectic penetration length and its evolution with ϕ, we employed a static method using the observation of controlled defects (a « Cano wedge » [6] experiment), recently adapted and performed by F. Nallet and J. Prost on conventional lyotropic swollen smectic phases [7].

2. Principle of the experiment.

The method is based on the analysis of the dislocation network exhibited by a smectic confined in a cell of varying thickness (the so-called Cano wedge). It has been shown that, in swollen lyotropic phases, the organization of the dislocations is not trivial and depends strongly on λ [7].

The static elasticity of a smectic is expressed by the free energy per unit volume [5, 8] :

$$f = \frac{1}{2}\bar{B}(\partial_z u)^2 + \frac{1}{2}Kc^2 + \frac{1}{2}\bar{K}g \tag{2}$$

where u is the displacement of each layer from its equilibrium situation, and c and g the mean and Gaussian curvatures of the layers, respectively. K is the mean curvature constant of the smectic and is related to the curvature constant κ of the lyotropic constituent membranes by $K = \kappa/e$ [9, 10] where e is the smectic periodicity. $\bar{B}$ is the compressibility at constant surfactant potential [11] (and, in the case of doped phases, at constant particle chemical potential [12]). $\bar{K}$ is the Gaussian curvature constant of the system, related to saddle-splay deformations [8, 13].

When a smectic mesophase is confined in a glass cell presenting a thickness gradient, it has to satisfy two conditions :

- A boundary condition of « homeotropic » orientation, i.e. with the layers parallel to the limiting glass walls. This preferential orientation, which is a general trend in lyotropic smectics, is specially enhanced in the doped phases [2] ;
- A condition of minimal free energy (Eq. (2)), which sets the periodicity to an equilibrium value e.

The phase adapts to the thickness gradient both by creating edge dislocations, each one involving a number (what we will call the « Burgers number ») b of layers which is not necessarily equal to 1, and by adjusting e between two adjacent dislocations. The distribution for the dislocations was calculated in reference [7] for an axial symmetry, in the case where the cell is produced by a spherical lens in contact with a plane. Two main terms have to be taken into account :

1) The defect energy of each dislocation of Burgers vector be, due to the curvature of the layers in each dislocation (per unit length) [8, 14] :

$$\varepsilon_d = \frac{\pi}{2} K \operatorname{Ln} \frac{b}{2 b_c} \tag{3}$$

where b_c is a short-scale (or « core ») cut-off length. This energy favours the gathering of the layers in a few dislocations of large Burgers vector, in order to reduce the curvature energy (as the logarithmic dependence of b implies that $\varepsilon_d(b_1 + b_2) < \varepsilon_d(b_1) + \varepsilon_d(b_2)$) ([1]).

2) The wedge-confinement energy of the sample between two adjacent dislocations [7] :

$$\varepsilon_w = \frac{\bar{B} \ell^3}{12 R} \tag{4}$$

where ℓ is the distance between these two dislocations. This term has an effect opposed to ε_d as it tends to reduce the distance between dislocations, i.e. it favours a pattern of small Burgers vector dislocations. When $\bar{B}$ is large, as in thermotropic and in non-swollen lyotropic smectics, this term is preponderant and drives the behaviour of the smectic, so that only elementary ($b = 1$) dislocations are observed [15, 16].

Note that, in principle, the far-field energy ε_{ff} due to the deformation of the neighbouring layers outside the dislocations would have to be taken into account [8, 14], but this energy is linearly dependent on b ($\varepsilon_{ff} = \bar{B} \lambda be/2$), so that it does not affect the distribution of the dislocations (ε_{ff}/ℓ vanishes during the derivation).

Using the sample energy per horizontal unit surface of the dislocation array $(\varepsilon_w + \varepsilon_d)/\ell$, the authors of reference [7] determine b the value of the Burgers number that minimizes this energy at each distance r from the center. This operation leads to the implicit expression of b (where the values of b obtained increase with r) :

$$\frac{b^3}{r^3} \frac{R^2 e^3}{3 \pi \lambda^2} = \operatorname{Ln} \left(\frac{b}{2 b_c} \right) - 1 . \tag{5}$$

Since the geometry of the cell imposes the relation :

$$\ell(r) = Reb(r)/r \tag{6}$$

it is convenient to write (5) as :

$$\ell(r) = (3 \pi \lambda^2 R)^{1/3} \mathscr{L} \left(\frac{r}{r_0} \right) \tag{7}$$

where

$$r_0 = 5.44 \, e b_c \left(\frac{R^2}{3 \pi \lambda^2} \right)^{1/3} \tag{8}$$

([1]) The calculation omits a term due to the Gaussian curvature which exists in principle since the edge dislocations are not rectilinear but concentric in this geometry. The curved layers consequently bear a saddle-splay deformation, whose two principal curvature radii are be and r (the distance of the dislocation to the center of the cell as shown in Fig. 1) with $be \ll r$. As in the lamellar phase K is of the order of $\bar{K}$ [13], it is clear by comparing the two curvature terms in the free energy (Eq. (2)) that we may neglect the Gaussian contribution $\bar{K}/rbe$ towards the mean curvature term $K(1/r + 1/be)^2$ in the calculation of the defect energy.

and $\mathscr{L}(x)$ is the inverse of $g(y) = \frac{e^{y^3}}{y}$. Since we only consider here the $y \geq y_{min}$ branch of $g(y)$, where $y_{min} = 0.67$ and $x_{min} = g(y_{min}) = 2.01$ correspond to the minimum of the g function, $\mathscr{L}$ is uniquely defined.

It is important to note that $(\varepsilon_w + \varepsilon_d)/\ell$ cannot be minimized by a positive value of b when $x < x_{min}$, which corresponds to $r < r^* = r_0/2.01$; here the dislocations do not present a high enough Burgers number b to have their energy approximated by expression (3), which is valid only when the layers folded in the dislocations may be considered as a continuum [14]. Nallet and Prost proposed that, in this part of the cell, the Burgers vector stops varying, keeping in a « quenched b regime » the value $b_{min} = 7.54\, b_c$ that is reached at $r = r^*$. According to our experimental results, the quenched b regime does not always accurately describe the evolution of b near the center of the cell, and one usually observes a succession of plateaux corresponding to discrete decreasing values of b when r decreases below the domain of validity of (3). However, we may note that the theory of reference [7] applies to the behaviour of the dislocation pattern till the first plateau. We will then compare the experimental results with this model where it is valid, and we will interpret the smallest b values that do not fall into this description with a model using a discrete defect energy.

3. Studied system and materials.

Ferrosmectic phases and their structural features have been described in previous papers [1-3]. The system appears as a stack of lyotropic membranes, formed by a sodium dodecyl sulfate (SDS) and pentanol bilayer holding water. The weight ratio water/SDS is fixed at 2.5, which sets the membrane thickness $e_{membrane}$ at 5 nm. Between the membranes, the swelling solvent is a colloidal suspension of magnetic particles (average diameter 7 nm) in cyclohexane, or ferrofluid (« oil »). The phases are stable for a particle volume fraction ϕ up to 4 %. The periodicity $e = e_{membrane} + e_{oil}$ (e_{oil} being the thickness of the oil layers) varies between 20 and 40 nm ; it is driven by the ratio ϕ_{oil}/ϕ_{water} (volume fractions) and depends only weakly on ϕ [17].

The Cano cell is made of a plano-convex spherical glass lens (we used two curvature radii : R = 517 or 956 mm) set on a glass plane disc, the diameters of the two parts being equal to 5 cm. A drop of ferrosmectic phase is squeezed between the two parts (Fig. 1a), then the cell is sealed with cyanoacrylate glue in order to prevent evaporation. The phase is then annealed by heating it to the isotropic phase (the L_3 « sponge » phase), and slowly cooled down (0.2 °C/mn) to obtain homogeneous anchoring over the whole cell, with the layers parallel to the glass boundaries. This stage is the most delicate of the experiment, since the cyanoacrylate glue does not always mechanically resist the temperature increase (up to 60 to 80 °C). On correctly annealed samples, the observation under optical microscope shows concentric dislocations, laid in a very regular way (Fig. 1b). The position of each dislocation is plotted by positioning it in the eyepiece, and displacing the cell with a micrometic displacement stage. It is worth stressing that, as the particles absorb light strongly, these defects are not easily observable between crossed polarizers, and have to be observed with a strongly converging light. Using this method, it is possible to distinguish the dislocations even in thin regions. Moreover, the presence of the green-absorbing particles renders light quasi monochromatic and improves the contrast.

4. Data treatment.

The experiment provides directly the position (distance r to the centre) of each dislocation, pinpointed by its rank n in order to plot a $r(n)$ graph (Figs. 2a and 2b). The local slope of this

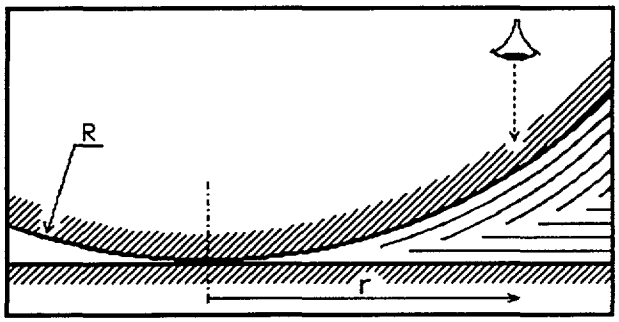

a)

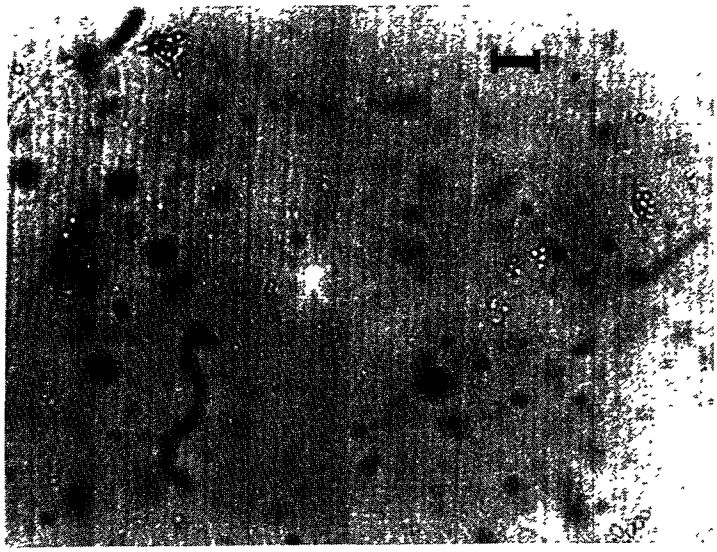

b)

Fig. 1. — a) Experimental set-up. Hatched parts : glass lens and plate ; b) optical microscopy picture of an array of dislocations ; bar = 0.1 mm.

graph is $\ell(r) = r(n+1) - r(n)$, and its theoretical expression (directly or by the mean of b) has been displayed in section 2. The theory gives ℓ *versus* r, and we want to compare it to our experimental data that are in the form $r(n)$:

In the low b region ($r < r^*$), as long as $b = b_{\min} = 7.54\, b_c$, the relation between r and n is simply :

$$r(n) = \sqrt{2\,Rneb_{\min} - (neb_{\min})^2}\,. \tag{9}$$

This regime is completely specified by the geometry of the cell and the $b_{\min}$ value, so that its shape does not depend on λ and appears as part of a concave down ellipse part. It crosses over through an inflexion point (at $r = r^*$, depending *via* r_0 on both parameters λ and b_c) to the convex « $\mathscr{L}$-regime » described hereafter, which is mainly dependent on λ.

For $r > r^*$, as the slope of the experimental curve varies quite slowly, we construct the theoretical curve by using the recurrence relation $r(n+1) = r(n) + \ell(r(n))$ where ℓ is calculated using equation (7) and proceeding to a numerical integration of ℓ. Since

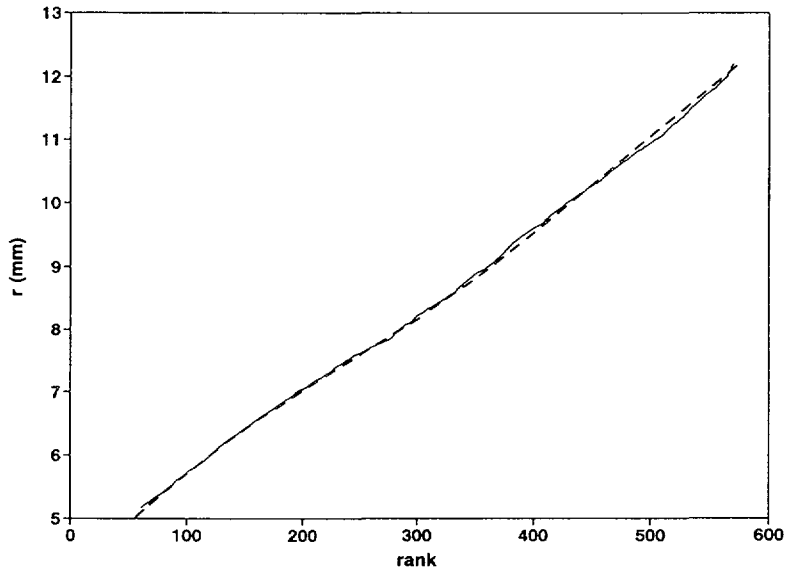

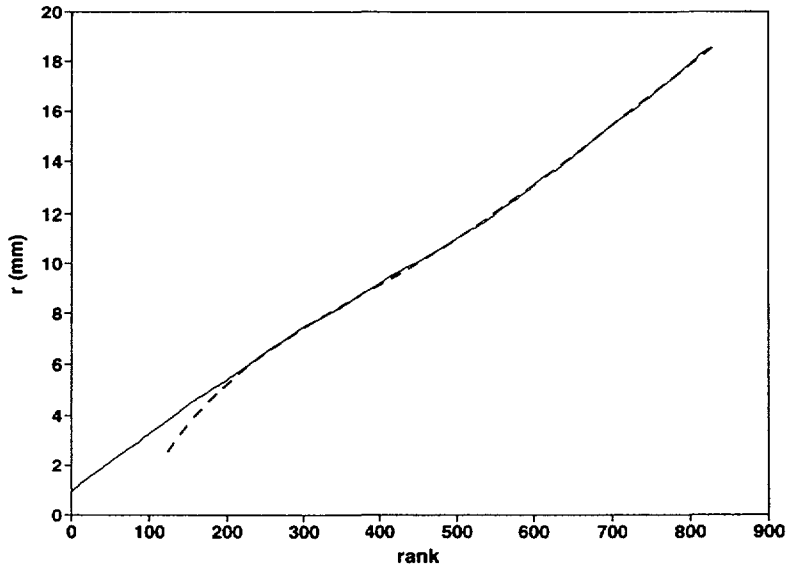

Fig. 2. — a) (——) : experimental $r(n)$ graph for $\phi_{oil}/\phi_{water} = 5.25$, $\phi = 2.8\ \%$ ($R = 517$ mm) ; this plot appears as a line because the dislocations are too close to be resolved on the graph ; (- - - - -) : The corresponding theoretical curve whose parameters are displayed in table I, and which provides $r^* = 7.9$ mm ; b) same set of curves for $\phi_{oil}/\phi_{water} = 4$, $\phi = 2.26\ \%$ ($R = 956$ mm). Here $r^* = 9.3$ mm ; at small r appears the discrepancy with the model of reference [7], discussed in section 2 and section 5.2 ; c) experiment of figure 2a : representation of the Burgers vector of each dislocation ($be = Ir/R$) *versus* r. The experimental uncertainty is emphasized by the use of the local slope of the experimental $r(n)$ points in the calculation of be. Thick line : theoretical curve with the parameters of table I ; note the cross over between the two regimes at $r = r^*$; d) Burgers representation for the experiment of figure 2b. The decrease of b at small r from the first plateau is observable even though its accuracy is not sufficient at this distance from the center to allow one to clearly distinguish the steps.

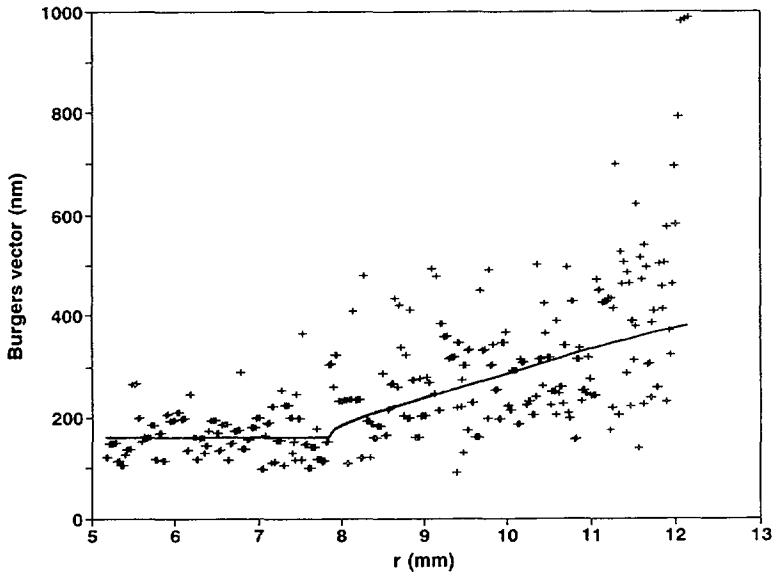

c)

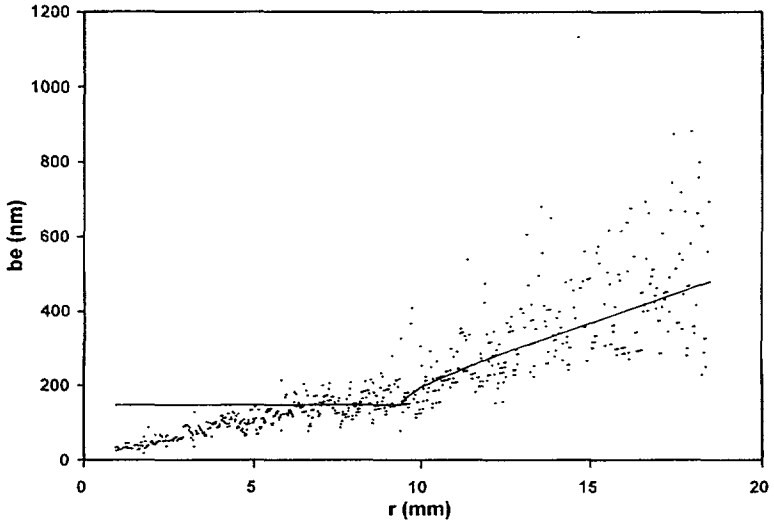

d)

Fig. 2 *(continued).*

$\mathscr{L}(x)$ cannot be expressed analytically, we approximate it numerically by the $\tilde{\mathscr{L}}(x)$ function, constructed in order to have the same value and slope for $x = x_{min}$ ($x_{min} = 2.01$ and $y_{min} = 0.67$) corresponding to the extremum of the g function defined in section 2 and to present a reasonable maximal square deviation about the $\mathscr{L}$ function :

$$\tilde{\mathscr{L}}(x) = x_{min} + (c \text{ Ln } (1 + a_1(x - y_{min}) + a_2(x - y_{min})^2) + a_3(x - y_{min})^3)^{\nu} \qquad (10)$$

with :

$$c = 206.94\ ;\quad a_1 = 4.903 \times 10^{-4}\ ;\quad a_2 = -4.298 \times 10^{-5}\ ;$$

$$a_3 = 3.749 \times 10^{-4}\ ;\quad \nu = 1/2.421\ .$$

For $x = r/r_0 < 11$ (which corresponds to $r < 22\,r^*$, and will appear as matching the experimental explored interval), the maximal square deviation between $\mathscr{L}$ and its approximated formula with the coefficients expressed here is less than 0.1 %. We thus use $\tilde{\mathscr{L}}$ instead of $\mathscr{L}$ when calculating the theoretical curve, and we determine λ and b_c for each experiment by adjusting them through a least squares method, for the two regimes at the same time.

We note that relation (5) shows the existence of a linear relation between b^3/r^3 and Ln b, far simpler than the complex relation between r and n that requires the use of the non-explicit function $\mathscr{L}$. We nevertheless do not work with this relation because it uses, through b, the finite difference $\ell = r(n+1) - r(n)$ of the experimental points, which is more sensitive to the experimental uncertainty than the $r(n)$ points. The variation of b with r (that is to be appreciated in Figs. 2c and 2d) is especially enhanced in b^3/r^3 and prevents its use in precise estimates.

In a few cases (indicated in Tab. I), it happened that the contact could not be perfectly achieved at the center of the cell, a state that is easily detectable as the ferrosmectics are strongly coloured. The modifications induced by a nonzero thickness at the center of the cell are calculated in the appendix. They lead to a lower value of r^*, easily understood by the fact that, at the same distance from the center, more layers buffer the gradient thickness. The effect of ε_w is then smaller, and may be counterbalanced by the unmodified ε_d nearer the center. The data are however to be treated in a way that is very similar to the others, as shown in the appendix.

Table I. — *Periodicity e : from* SANS *measurements of reference* [17].

ϕ_{oil}/ϕ_{water}	ϕ (%)	e (nm)	a (mm)	R (mm)	λ (nm)	b_c
5.25	0	25.0		517	51.3	0.49
8.5	0	38.0		956	74.2	0.90
5.25	1.13	26.4		956	53.7	1.55
5.25	1.13	26.4		517	40.7	0.85
8.5	1.13	40.1		956	66.5	0.62
4	2.26	22.3	0.004	956	38.0	0.91
5.25	2.26	27.8		956	40.5	0.80
8.5	2.26	42.3	0.02	956	46.4	0.68
4	2.8	22.8		956	28.5	0.85
5.25	2.8	28.5		956	28.6	0.73
5.25	2.8	28.5		517	28.4	0.78

5. Experimental results and determination of λ.

We studied the ferrosmectic phases for three ratios ϕ_{oil}/ϕ_{water} (4, 5.25 and 8.5) and three particle concentrations (1.13 %, 2.26 %, 2.8 %), and compared these to the undoped reference systems. The results are summarized in table I, that displays the values of λ and b_c for the different phases and experimental conditions.

5.1 CLASSICAL UNDOPED PHASES. — The Cano wedge experiment was first performed on undoped phases. As in the experiments of reference [7] performed on comparable phases, the dislocation pattern $r(n)$ observed presents a concave up part, and for smaller r the beginning of a concave down elliptical part, the whole being in accordance with the theoretical curve of section 4. We have measured λ for two ratios ϕ_{oil}/ϕ_{water} . 5.25 and 8.5. For sufficiently swollen phases, the values of λ are proportional to the periodicity e, as deduced from Helfrich's potential [9, 18] :

$$\lambda = \frac{8}{3\pi}\frac{\kappa}{kT}e\,. \tag{11}$$

We thus obtain an estimate of the curvature constant of the membrane in undoped cyclohexane phases : $\kappa \approx 2.4\ kT$, which is compatible with values obtained in analogous systems [18]. As this experiment is long and delicate, we did not measure λ for $\phi_{oil}/\phi_{water} = 4$, and extrapolated it linearly to 41 nm.

5.2 FERROSMECTICS. — In the doped phases the possibility of distinguishing the defects in thin regions, near the center of the cell, allows us to count a large number of dislocations, up to 800 for some experiments. In these phases, the concave up $\mathscr{L}$-regime is also observed, followed by a concave down part when approaching the center (Figs. 2a, b). On the $be(r)$ curve, one may observe that the evolution of the Burgers vector with r effectively exhibits a zone where b is constant, following the $\mathscr{L}$-regime where b decreases (Fig. 2c). However, in most of the experiments, this plateau does not extend down to the center and gives way to a succession of decreasing steps (Fig. 2d). This invalidates the hypothesis of a quenched b regime over the whole range $0 < r < r^*$ We will nevertheless determine λ according to reference [7] in the range where it is valid, as discussed in section 2. The values of λ are displayed in figure 3, as a function of ϕ for different ϕ_{oil}/ϕ_{water}. Roughly, we see that λ first remains constant at very small ϕ, then starts decreasing with increasing ϕ, and that this effect is more pronounced for large values of the periodicity e. As concerns b_c, the values obtained when determinating λ (Tab. I) are close to 0.8. This corresponds to a core zone that is somewhat smaller than a layer, which is a reasonable order of magnitude.

About the approximation proposed in section 4, we note that $r < 22\ r_0$ in all cases ; this confirms the validity of using $\hat{\mathscr{L}}$ in place of $\mathscr{L}$ in the data treatment.

6. Interpretation of the very small Burgers vector dislocations.

In the vicinity of the center, dislocations of very small Burgers number ($b < 5$) have been observed. In one phase, with a high concentration of particles ($\phi = 2.8\ \%$), the dislocations could be distinguished very close to the center (up to $r = 1$ mm). When plotting the Burgers vector be as a function of r, we observe two well-defined plateaux, at $be = 37$ nm and $be = 70$ nm (Fig. 4). The measurement of $e = 35.0$ nm by X-ray scattering shows that the first plateau corresponds to elementary dislocations ($b = 1$), and the second one to $b = 2$. The dislocations, which are even harder to distinguish in this case than in the « usual » cases, get

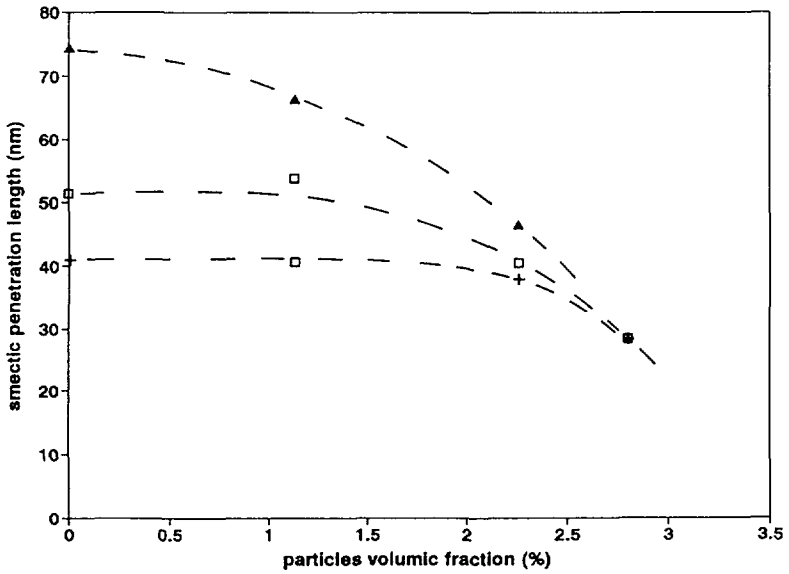

Fig. 3. — λ *versus* ϕ for different swelling ratios ; the lines are a guide for the eyes. (+) : $\phi_{oil}/\phi_{water} = 4$; (□) : $\phi_{oil}/\phi_{water} = 5.25$; (▲) : $\phi_{oil}/\phi_{water} = 8.5$.

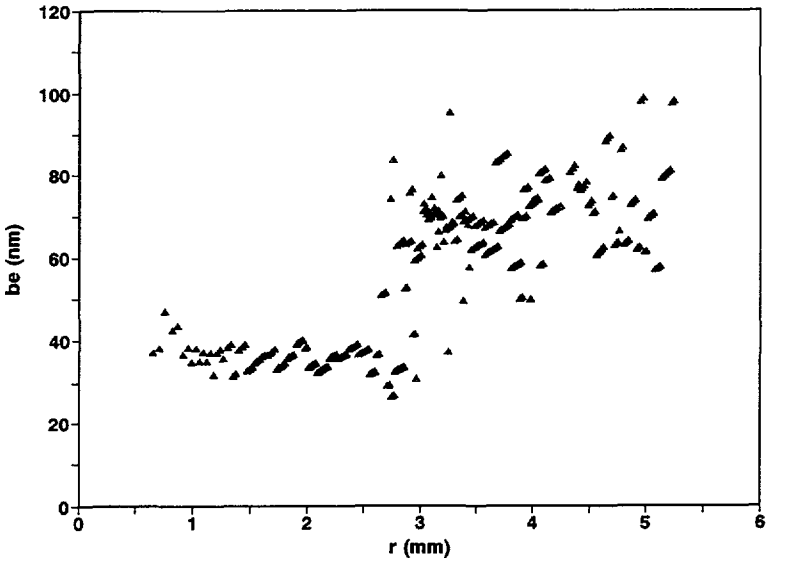

Fig. 4. — $\phi = 2.8$ % and $e = 35$ nm : Burgers vector (here $R = 956$ mm, and $r^* = 2.9$ mm). As the dislocations have a very poor contrast, the positions were sometimes counted by blocks ; this gathers the points into inclined stripes. For larger r, the defects are hardly perceptible and the dispersion of the points increases.

closer when going away from the center, and at $r > \approx 5$ mm become gradually impossible to separate from each other by optical microscopy.

In the region of observation, the $\mathscr{L}$-description, for which the layers implied in the dislocations are approximated as a continuum, is obviously inaccurate, so we will use a discrete model to obtain λ. One may assert that the radius r^* that separates the $b = 1$ and $b = 2$ regions corresponds to equal values of the total energy per unit surface, $\varepsilon/\ell = (\varepsilon_w + \varepsilon_d)/\ell$, at $b = 1$ and $b = 2$. The limit between the two Burgers vectors results then from the competition between the defect and wedge-confinement energies, just as in section 2 and r^* obeys :

$$\bar{B}Re^2/12\, r^{*2} + (r^*/Re)\, \varepsilon_d(b = 1) = 2\, \bar{B}Re^2/3\, r^{*2} + (2\, r^*/Re)\, \varepsilon_d(b = 2)\,. \tag{12}$$

We deduce then :

$$\lambda = \sqrt{\frac{R^2\, e}{4\, r^{*3}(\varepsilon_d(b = 1)/K - \varepsilon_d(b = 2)/2\, K)}}\, e\,. \tag{13}$$

In this equation, $\varepsilon_d(b = 1)$ and $\varepsilon_d(b = 2)$ can be calculated with microscopic models, as the sum of the discrete curvature energies of the bi- or monolayers involved in these dislocations.

We may consider that the structure of a $b = 2$ dislocation involves the folding up of a bilayer with a curvature radius $e/2$, as shown in figure 5a. We then have :

$$\varepsilon_d(b = 2) = \pi\kappa/e = \pi K\,. \tag{14}$$

For $b = 1$, two models are conceivable. In the simpler one (displayed in Fig. 5b), the elementary dislocation is achieved *via* the ending of a bilayer, ending which is obtained by folding up the constituent monolayers. As the curvature constant of the monolayer is $\kappa_{mono} = \kappa/2 = K/2\, e$, and the curvature radius in this situation is of the order $\delta/2$ (δ being the membrane thickness), we get :

$$\varepsilon_{d_{end}}(b = 1) = \frac{\pi}{2} Ke/\delta\,. \tag{15}$$

In our case, the value of $\varepsilon_{d_{end}}(b = 1)$ is 10.7 K. With the two different cells $R = 956$ and $R = 517$ mm (respectively $r^* = 2.9$ and $r^* = 1.9$ mm), we obtain through equation (13) : $\lambda_{end} = 6.4$ and 6.5 nm.

The other way to get $b = 1$ is the connection of two bilayers, as shown in figure 5c. In this configuration, we see that the curvature energy is the same as that of a $b = 2$ defect, except that in the connection region a portion of monolayer of curvature radius $\dfrac{e + \delta}{2}$ is replaced by two parts with an *a priori* undetermined curvature radius r. Simple geometric considerations impose :

$$\varepsilon_{d_{conn}}(b = 1) = \varepsilon_d(b = 2) + \kappa_{mono}\left(\frac{\theta}{r} - \frac{\pi - 2\,\theta}{e + \delta}\right) \tag{16}$$

with

$$\theta = \text{Arccos}\left(\frac{r + \delta/2}{r + (e + \delta)/2}\right).$$

If we assume that the connection region has a size comparable to the membrane thickness (i.e. $x = 5$ nm), the r value is imposed through the geometric relation :

$$x = (r + (e + \delta)/2)\sin\theta - (e + \delta)/2\,.$$

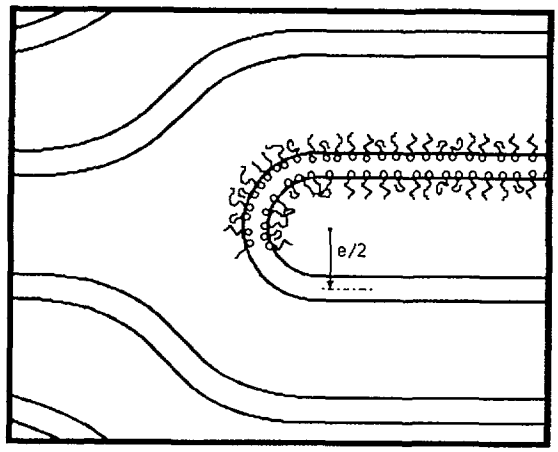

a)

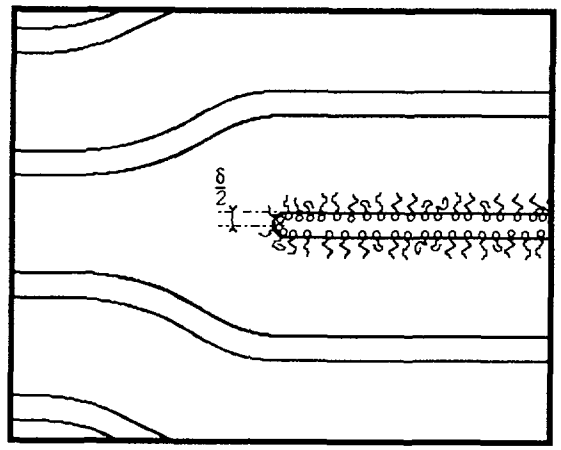

b)

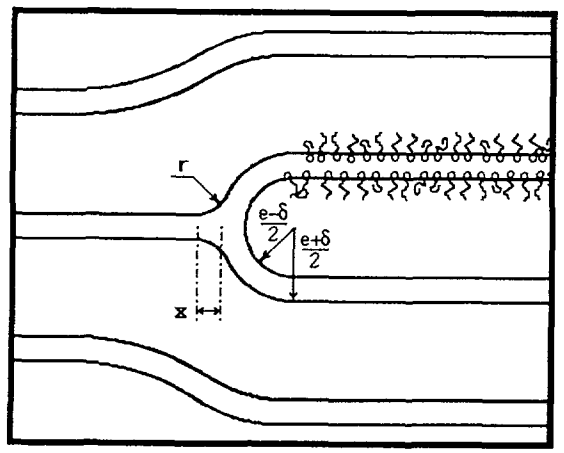

c)

Fig. 5. — a) Microscopic model for a $b = 2$ dislocation ; b) ending bilayer model for a $b = 1$ dislocation ; c) model with two connecting bilayers for a $b = 1$ dislocation.

Here, $x = 5$ nm imposes $r = 6.6$ nm, and consequently $\varepsilon_{d_{conn}}(b = 1) = 5.9\ K$. The two values of λ_{conn} deduced from the two different experiments are then 9.2 and 9.4 nm, which are higher than those determined using the terminating bilayer model.

We see that the determination of λ depends on the model used (the second one being the more plausible, as it leads to a lesser dislocation energy), but in any case the value obtained is significantly smaller than the smectic penetration lengths of phases less swollen or with smaller particle volume fraction. The reduction in λ is then particularly strong in this extreme region. We also note that such a small value of λ explains *a posteriori* the fact that we could not, in this experiment, observe the dislocations outside a very central zone, as they got closer and faded away when getting away from the center. Effectively, a small smectic penetration length (« hard » smectic) makes it easier to curve the layers in separate dislocations than to adapt to the thickness gradient between the dislocations : the Burgers vector will then increase more slowly with r than in « soft smectics » and the dislocations will be closer. This has two consequences : first, the dislocations involving a few layers show poor contrast and are more difficult to see in the thick highly light-absorbing regions of the cell. Secondly, low values of b also reduce ℓ and may have it drop below the spatial resolution of the microscope.

7. Discussion.

The most remarkable feature is that, at constant swelling ratio, there is no variation of the penetration length λ with the particle volume fraction ϕ when ϕ is small ($\phi < 1$ to 2 %). If we recall that the variations of the elastic bending and compression constants K and $\bar{B}$ with ϕ are correlated with λ values through $\lambda = \sqrt{K/\bar{B}}$, we may deduce from the constancy of λ at small ϕ that K and $\bar{B}$ vary in the same way, if they vary with ϕ. These results are to be compared to those of Small-Angle Neutron Scattering (SANS) where the spectra of the ferrosmectics — even for weak particle concentration — are totally different from those of undoped phases, the qualitative analysis indicating that the quantity $K\bar{B}$ is strongly enhanced as soon as particles are introduced [17]. Consequently, both $\bar{B}$ and K, (that vary separately like $\sqrt{K\bar{B}}$ as the λ measurements show that they have both a similar evolution) have to increase rapidly with ϕ at small particle concentration. Together with SANS experiments, we have here the first experimental clue on the variation of K, which increases strongly as soon as the phase is doped.

It is interesting to discuss this last result from the point of view of the mechanisms that stabilize the ferrosmectic phases. In a classical swollen system, the long-distance repulsive interactions are due to the entropically reduced fluctuations of confined membranes (Helfrich-type repulsion). This is the case for $\phi = 0$, and the expression of the compression constant is [9, 18] :

$$\bar{B} = \frac{9\ \pi^2 (kT)^2}{64\ \kappa e^3} \tag{17}$$

Thus at constant interlayer distance, $K = \kappa/e$ and $\bar{B}$ should be inversely proportional. This is not compatible with the simultaneous increase of K and $\bar{B}$ that we observe. In agreement with SANS results, the present experiment shows that there is a supplementary stabilization process in the ferrosmectic phase that adds to the steric repulsion between fluctuating membranes, and enhances $\bar{B}$ compared to a Helfrich-type behaviour.

Let us now consider what happens over the whole range of ϕ, when λ cannot be considered as constant : λ decreases for $\phi > 1$ to 2 %, indicating that $\bar{B}$ eventually increases more rapidly

than K. We may suggest that the evolution of λ is mainly due to a slowing down of the K increase ; this would correspond to a strong effect on the stiffness of the membrane as soon as the particles are introduced, followed by a saturation phenomenon when the total concentration of particles becomes large. On the contrary, $\bar{B}$, which is related to the intermembranar repulsion, would keep increasing when the particles are added between the layers.

We can look more quantitatively at the evolution of λ, by observing the curves in figure 3 : the decrease of λ starts all the sooner and is all the more significant as the phase is more swollen. Thus ϕ and ϕ_{oil}/ϕ_{water} act on λ in a similar way. This equivalence between highly swollen phases with few particles and less swollen phases that are more concentrated, may be expressed in terms of characteristic distances : e for ϕ_{oil}/ϕ_{water} and d_p (mean distance between the particles into the layers) for ϕ. For the present experiment, the nature of the evolution of λ shifts for a typical value of e/d_p, of order of unity. This can be compared with the observations of Ponsinet *et al.* [17] in neutron scattering, where a cross-over in the behaviour of the main SANS features (position, intensity of the peaks) is driven by e/d_p, the threshold value being about half that seen here. The ratio e/d_p is thus a key parameter, whose role is yet to be completely clarified.

8. Conclusion.

We have measured the smectic penetration length of doped phases through a varying thickness cell method that is very well suited to the material studied, owing to its optical and spontaneous orientation features. The limit of the model, initially built for undoped phases by Nallet and Prost, has been delineated when the confining of the smectic is more intense, in the central part of the cell. Outside this limit, in the thinner region, we have observed elementary edge dislocations that had not been seen in this type of experiment with conventional swollen lyotropic phases.

The measurements carried out show that the doping of the phases decreases λ, which means that a deformation imposed on the smectic requires a greater distance to attenuate. This supports the intuitive idea that the presence of solid particles between the lyotropic membranes hardens the smectic, and justifies the appearance of small Burgers dislocations. As the variation of λ is very weak for small ϕ values, this study coupled with previous SANS observations shows that $\bar{B}$ and K have a concomitant variation in this particle concentration range. This is inconsistent with the classical interpretation where swollen smectics are stabilized by the steric hindrance between fluctuating membranes, and strengthens the conclusion obtained from SANS studies of the existence of supplementary interactions in these doped systems. Ultimately, we get information on the sense of variation of K, that increases strongly as soon as particles are inserted in the phases, and we foresee a saturation effect of the membranes by the particles on the bending elasticity at high particle concentration.

Acknowledgements.

For this work we are greatly indebted to F. Nallet for his friendly help and encouragement, and we warmly thank M. Kléman and J. Prost for discussions and advice.

Appendix.

Calculation of the effect of a finite thickness at the center of the cell.

A nonzero thickness a (measurable by transmission) at the center of the cell does affect directly only ε_w. If we integrate the compression of the layers (term $\frac{1}{2}\bar{B}(\partial_z u)^2$ in Eq. (2)) over a

thickness $a + r^2/(2R)$ instead of $r^2/(2R)$, following the way of reference [7], and write conveniently all terms in ℓ instead of b (which is possible as the geometric relation (6) shows the proportionality, at a given r, between b and ℓ), the calculation leads to :

$$\varepsilon_w(a) - \varepsilon_w(0) = \bar{B}\left(-\frac{\ell a}{2} + \bar{h}^2 \sqrt{\frac{R}{2a}} \left(\text{Arctg} \frac{\sqrt{2Ra}}{r - \ell/2} - \text{Arctg} \frac{\sqrt{2Ra}}{r + \ell/2} \right) - \frac{\ell r^2}{4R} \right)$$

where :

$$\bar{h} = a + \frac{r^2 + \ell^2/4}{2R}$$

Expanding the Arctg in series in $\ell/2r$ leads to :

$$\sqrt{\frac{R}{2a}} \left(\text{Arctg} \frac{\sqrt{2Ra}}{r - \ell/2} - \text{Arctg} \frac{\sqrt{2Ra}}{r + \ell/2} \right) = \frac{2R}{r(1+u)} \frac{\ell}{2r} + \frac{2R(1 - u/3)}{r(1+u)^3} \left(\frac{\ell}{2r} \right)^3 + O\left(\left(\frac{\ell}{2r} \right)^5 \right)$$

with :

$$u = \frac{a}{r^2/2R}$$

As we are only interested in the derivation of ε_w/ℓ, we will not retain the terms of $\varepsilon_w(a) - \varepsilon_w(0)$ that are linear in ℓ, vanishing with the derivation. The only terms that have to be taken into consideration are then the ℓ^3 ones ; they may be written as $\frac{\bar{B}\ell^3}{12R} f(u)$, where :

$$f(u) = \frac{(1 + 2u)(3 - u)}{4(1 + u)^3} - \frac{3}{4}.$$

The expression of $\varepsilon/\ell = (\varepsilon_w + \varepsilon_d)/\ell$ is then hardly different from the case $a = 0$: in order to take the finite value of a into account, the only modification is to write $\bar{B}(1 + f(u))$ instead of $\bar{B}$. As $f(u) = F(r)$ is independent of ℓ (and, consequently, of b), the minimization of $(\varepsilon_w + \varepsilon_d)/\ell$ with respect to b treated in section 2 remains valid. The calculation shows that the only correction to the following operations is to replace λ by $\lambda (1 + F(r))^{-1/2}$ in equations (7) and (8) when calculating $\ell(r)$ at each point. In terms of a $r(n)$ representation, this still corresponds to a convex ellipse fragment, with no incidence on the b_{min} value, followed from r^* by a concave part. However r^* is decreased, as the relation that defines it is now :

$$r^* = (1 + F(r^*)) x_{min}\, 5.44\, eb_c \left(\frac{R^2}{3\pi\lambda^2} \right)^{1/3} \quad \text{with} \quad F(r^*) < 0 .$$

The inflexion point at r^* then gets closer to thinner zones of the cell when the two constituting parts are not exactly brought into contact.

References

[1] Fabre P., Casagrande C., Veyssié M., Cabuil V., Massart R., *Phys. Rev. Lett.* **5** (1990) 64.
[2] Quilliet C., Fabre P., Cabuil V., *J. Phys. Chem.* **97** (1993) 287.
[3] Dabadie J. C., Fabre P., Veyssié M., Cabuil V., Massart R., *J. Phys. Condens. Matter.* **2** (1990) SA291.
[4] See for example the review article of Roux D., Milner S., Nallet F., to be published in Amphiphilic systems, Modern ideas, W. Gelbart, A. Ben Shaul, D. Roux Eds. (Springer Verlag) and references therein ;
Bassereau P., Appell J., Marignan J., *J. Phys. II France* **2** (1992) 1257 ;
Kékicheff P., Richetti P., Christenson H. K., *Langmuir* **7** (1991) 1874.
[5] de Gennes P. G., Physics of liquid crystals (Clarendon Press, Oxford, 1974).
[6] Cano R., Chatelain P., *C.R. Acad. Sci. Paris* **253** (1961) 1815/2081.
[7] Nallet F., Prost J., *Europhys. Lett.* **4** (1987) 307.
[8] Kleman M., *Rep. Prog. Phys.* **52** (1989) 555.
[9] Helfrich W. Z., *Naturforsch.* **33A** (1978) 305.
[10] Golubovic L., Lubensky T. C., *Phys. Rev. B* **39** (1989) 12110.
[11] Brochard F., de Gennes P. G., *Pramana* **1** (1975) 1.
[12] Nallet F., Roux D., Quilliet C., Fabre P., Milner S., to be published.
[13] Porte G., Appell J., Bassereau P., Marignan J., *J. Phys. France* **50** (1989) 1335.
[14] Friedel J., Dislocations (Pergamon Press, 1964).
[15] Meyer R. B., Stebler B., Lagerwall S. T., *Phys. Rev. Lett.* **41** (1978) 1393.
[16] Chan W. K., Webb W. W., *J. Phys. France* **42** (1981) 1007.
[17] Ponsinet V., Fabre P., Veyssié M., Auvray L., *J. Phys. II* **3** (1993) 1021.
[18] Nallet F., Roux D., Prost J., *J. Phys. France* **50** (1989) 3147.